Chemical Engineering Journal 396 (2020) 125208

Contents lists available at ScienceDirect

Chemical Engineering Journal

journal homepage: www.elsevier.com/locate/cej

Red shift properties, crystal field theory and nephelauxetic effect on Mn^{4+}-doped $SrMgAl_{10-y}Ga_yO_{17}$ red phosphor for plant growth LED light

Simin Gu[a,b,1], Mao Xia[a,b,1], Cheng Zhou[a], Zihui Kong[a], Maxim S. Molokeev[c,d], Li Liu[e,*], Wai-Yeung Wong[f,*], Zhi Zhou[a,b,*]

[a] School of Chemistry and Materials Science, Hunan Agricultural University, Changsha 410128, PR China
[b] Hunan Optical Agriculture Engineering Technology Research Center, Changsha 410128, PR China
[c] Laboratory of Crystal Physics, Kirensky Institute of Physics, Federal Research Center KSC SB RAS, Krasnoyarsk 660036, Russia
[d] Siberian Federal University, Krasnoyarsk 660041, Russia
[e] Hubei Collaborative Innovation Center for Advanced Organic Chemical Materials, Ministry of Education Key Laboratory for the Synthesis and Application of Organic Functional Molecules, School of Chemistry and Chemical Engineering, Hubei University, Wuhan 430062, PR China
[f] Department of Applied Biology and Chemical Technology, The Hong Kong Polytechnic University, Hung Hom, Hong Kong, PR China

HIGHLIGHTS

- A novel Mn^{4+}-doped $SrMgAl_{10-y}Ga_yO_{17}$ red phosphor with red shift and improved luminescence properties.
- Crystal field theory and nephelauxetic effect are employed to explain the red shift in luminescence spectra.
- The phosphor has potential application on plant growth LED light.

GRAPHICAL ABSTRACT

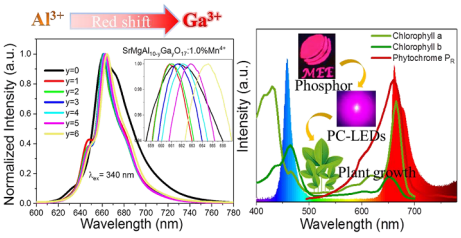

ARTICLE INFO

Keywords:
Red shift
Crystal field theory
Nephelauxetic effect
$SrMgAl_{10-y}Ga_yO_{17}$: Mn^{4+}
Plant growth LED light

ABSTRACT

The discovery of novel Mn^{4+}-doped oxide red phosphor with suitable spectrum for plant growth is a hot issue in the recent years due to the characteristic red photoluminescence of $^2E_g \rightarrow {}^4A_2$ transition in Mn^{4+} ions. Generally, the emission position of Mn^{4+} is hard to tune because of specific crystal field in most phosphors. In this work, tunable luminescence property with obvious red shift in the spectra is observed in the Mn^{4+}-doped $SrMgAl_{10-y}Ga_yO_{17}$ red phosphor via simple substitution of Ga^{3+} for Al^{3+}, and crystal field theory and nephelauxetic effect are employed to explain this phenomenon. Meanwhile, the Ga^{3+} dopant changes the shape of the spectra because Ga^{3+} dopant guides the replacement site of Mn^{4+} and changes the luminescence center. Improved emission intensity is obtained because appropriate Ga^{3+} doping leads to larger band gap and reduces non-radiative transitions. Phosphor-converted LED (pc-LED) devices fabricated with blue chip (470 nm) and the as-obtained $SrMgAl_{10-y}Ga_yO_{17}$:1.0%Mn^{4+} phosphors emit bright blue and red light, which fit the absorption regions of plant pigments well, thus $SrMgAl_{10-y}Ga_yO_{17}$:Mn^{4+} phosphor can be a candidate for plant growth LED light.

* Corresponding authors at: School of Chemistry and Materials Science, Hunan Agricultural University, Changsha 410128, PR China (Z. Zhou).
E-mail addresses: liulihubei@hubu.edu.cn (L. Liu), wai-yeung.wong@polyu.edu.hk (W.-Y. Wong), zhouzhi@hunau.edu.cn (Z. Zhou).
[1] Simin Gu and Mao Xia contributed equally to this work.

https://doi.org/10.1016/j.cej.2020.125208
Received 19 March 2020; Received in revised form 20 April 2020; Accepted 23 April 2020
Available online 25 April 2020
1385-8947/

1. Introduction

Plant cultivation plays an important role in agricultural production. Conventional agriculture suffers from harsh environment such as frost, cloudy weather, droughts and rainstorms, resulting in a reduced yield, which cannot satisfy people's needs. In recent years, indoor plant cultivation (IPC) has caused a lot of concern for constructing a suitable and stable environment for plant growth. Light source is an essential condition in the growth process of all plants including branching, flowering, and fruiting [1-3]. Light energy can be converted into chemical energy by photosynthesis of plant pigments. Chlorophyll *A*, chlorophyll *B*, phytochrome P_R and phytochrome P_{FR} are four main plant pigments which mainly absorb blue (400–500 nm), red (600–700 nm) and far-red (700–780 nm) lights. The traditional light sources for indoor plant cultivation are incandescent lamps, high voltage halogen lamps and xenon lamps, which suffer from many disadvantages such as high energy consumption, short lifetime and spectral mismatch. Therefore, benefit from characteristic merits of energy saving, long lifetime, spectral match and environment friendliness, phosphor-converted light-emitting-diode (pc-LED) has gradually been widely used in IPC. As a light-conversion material, phosphors play an indispensable role in LED devices which directly determine the photoluminescence properties, so it is important to design and synthesize the phosphors with proper spectral emission and bright photoluminescence [4-6].

Based on this fact, many phosphors have been investigated and discussed to fulfil the light requirements of plant growth. Red phosphors are the ideal material for plant growth LED light because red emission is beneficial in promoting plant growth and biomass accumulation. Meanwhile, red phosphors also have wide application in white light-emitting diodes [7-10]. Nowadays, the commercial phosphor $Y_3Al_5O_{12}:Ce^{3+}$ widespread used in white LEDs is not suitable for plant growth LEDs because of the mismatched spectral bands [11,12]. The main red phosphor Eu^{2+}-doped nitrides likes $(Ca,Sr)AlSiN_3:Eu^{2+}$ [13-15] and $(Ca,Sr)_2Si_5N_8:Eu^{2+}$ [16,17] suffer from severe synthetic conditions with high temperature (greater than1800°C) and high pressure in reductive atmosphere. The critical preparation requirement increases the cost of the product and limits their large-scale use in agricultural industry. Another red phosphor is Mn^{4+}-doped fluoride, such as $K_2TiF_6:Mn^{4+}$ [18] and $K_2SiF_6:Mn^{4+}$ [19]. Preparation of these materials often need HF while it is harmful to the environment, and they are unstable that easily decompose in moist environment because of the existence of $[MnF_6]^{2-}$ groups. As an alternative, Mn^{4+}-doped oxides have received extensive attention for series of advantages such as attractive photoluminescence properties, high stability, low cost and eco-friendliness [20,21]. New types of Mn^{4+}-doped oxides such as $SrLaAlO_4$ [22], La_2LiSbO_6 [23], Gd_2ZnTiO_6 [24], $Ca_{14}(Ga/Al)_{10}Zn_6O_{35}$ [25,26] have been reported for plant cultivation in recent years. Mn^{4+}-activated oxide phosphors can usually be excited by commercial blue and near ultraviolet chips because they have large photoluminescence excitation spectra ranging from 220 to 580 nm, and the emission band of these phosphors is located at the red and far-red regions from the characteristic $^2E_g \rightarrow {}^4A_2$ transitions of Mn^{4+}. Nonetheless, the emission position of Mn^{4+} in these matrixes is hard to tune to match the absorption of plant pigments better, so it still needs a novel matrix or method to develop red phosphors with more suitable spectrum for plant growth LED light.

Impurity doping plays a key role on the discovery of Mn^{4+}-doped oxides as red phosphors. It can be constructed easily through the substitution between elements in one main group, because these ions usually have similar ionic radius, analogical structure and electronegativity alike. Zhao *et al.* [27] and Zhou *et al.* [28] reported that the lattice site can be adjusted by replacing Ga^{3+} with Al^{3+} in $Ca_{14}Ga_{10-x}Al_xZn_6O_{35}$ phosphor, lead to an enhancement on photoluminescence intensity and quantum efficiency of the samples. Analogously, Qiao *et al.* reported a single-phase $(Ca_{9-x}Sr_x)MgK(PO_4)_7:Eu^{2+}$ phosphor with white light by adjusting the compositions and multiple activator sites, which show a significant shift and improvement on the photoluminescence spectra via Sr^{2+} replace Ca^{2+} [29]. Similar enhanced and tunable luminescence performances in $Lu_{3-x}Y_xAl_5O_{12}:Mn^{4+}$ red phosphor can also be explained in details due to the substitution of Y^{3+} for Lu^{3+} [30]. Taking the inspiration from these literatures, we assumed Ga^{3+} to replace Al^{3+} in $SrMgAl_{10}O_{17}:Mn^{4+}$ phosphor to improve luminescence properties. As far as we know, no similar literature has been reported.

In this study, a novel Mn^{4+}-doped $SrMgAl_{10-y}Ga_yO_{17}$ red phosphor with tunable and improved luminescence properties is discovered. The samples were prepared through high-temperature solid-state method in atmospheric environment. The phase structure, photoluminescence (PL) and photoluminescence excitation (PLE) spectra, absorption spectra, quantum efficiency, lifetime decay curves and electroluminescence properties are investigated in detail. Finally, series of LED devices combined with blue chips and the as-obtained phosphors show bright blue and red emissions which match the plant absorption spectrum well, indicates this phosphor can be a candidate for indoor plant growth light.

2. Experimental section

The raw materials were $SrCO_3$ (99.99%), MgO (99.99%), Al_2O_3 (99.99%), Ga_2O_3 (99.99%) and $MnCO_3$ (99.99%), which were bought from Aladdin without further purification. Different contents of H_3BO_3 (AR) (1, 2, 3, 4, 5% wt) acted as flux in the reaction process. All reagents were weighed following the stoichiometric ratio and put into an agate mortar, dropped with a certain amount of absolute ethyl alcohol. These powders were ground for 30 min to mix up uniformly then transferred into corundum crucibles. They were put into a tube furnace preheated at 800 °C for 2 h and sintered at 1500 °C in ambient atmosphere for 5 h with a heating rate of 5 °C/min in the whole process. All samples were cooled down to room temperature naturally and then reground to fine powders. Finally, the $SrMgAl_{10}O_{17}:xMn^{4+}$ (x = 0.1%, 0.3%, 0.5%, 1.0%, 1.5%, 2.0%) and $SrMgAl_{10-y}Ga_yO_{17}:1.0\%Mn^{4+}$ (y = 1, 2, 3, 4, 5, 6) samples were obtained.

The X-ray powder diffraction (XRD) patterns were measured ranging from 10° to 80° by a diffractometer (D/SHIMADZU-6000, Japan) which equipped with Cu-Ka radiation (λ = 1.5406 Å). The scanning rate was 6°/min and operating voltage and current were 40 kV and 40 mA. F-4700 fluorescence spectrophotometer (Hitachi, Japan) was used to obtain the photoluminescence excitation (PLE) and photoluminescence (PL) spectra with a 150 W Xe lamp as the excitation lamp. The UV–vis absorption spectra were tested on U-3310 spectrophotometer (Hitachi, Japan). Temperature-dependent PL spectra were measured using F-7000 Spectro-photometer (Hitachi, Japan) by changing the testing temperature from 298 K to 473 K. FLS 1000 fluorescence spectrometer (Edinburgh, UK) was used to get the lifetime curves and quantum efficiency. The photographs of sample were taken by Sony A6400 camera.

The LED devices were fabricated using two-component epoxy resin (Kraft K-9761) to encapsulate the as-obtained phosphors on the blue chip. The transparent resin A and B was mixed with the weight rate of 2:1, then the well-mixed resin and phosphor further mixed with the weight ration changed from 1:1 to 1:3. An ATA-500 measurement system (Everfine, China) was used to carry out the luminescence spectra of these LED devices.

3. Results and discussion

3.1. Structure and phase characterization

First of all, H_3BO_3 was chosen as flux in the synthesis process, as shown in Fig. S1 (a). The XRD pattern of samples exhibit impurity phase of $SrAl_2O_4$ before the content of H_3BO_3 is below 2 wt%, and after that the XRD represent pure phase of $SrMgAl_{10}O_{17}$ with the standard card of

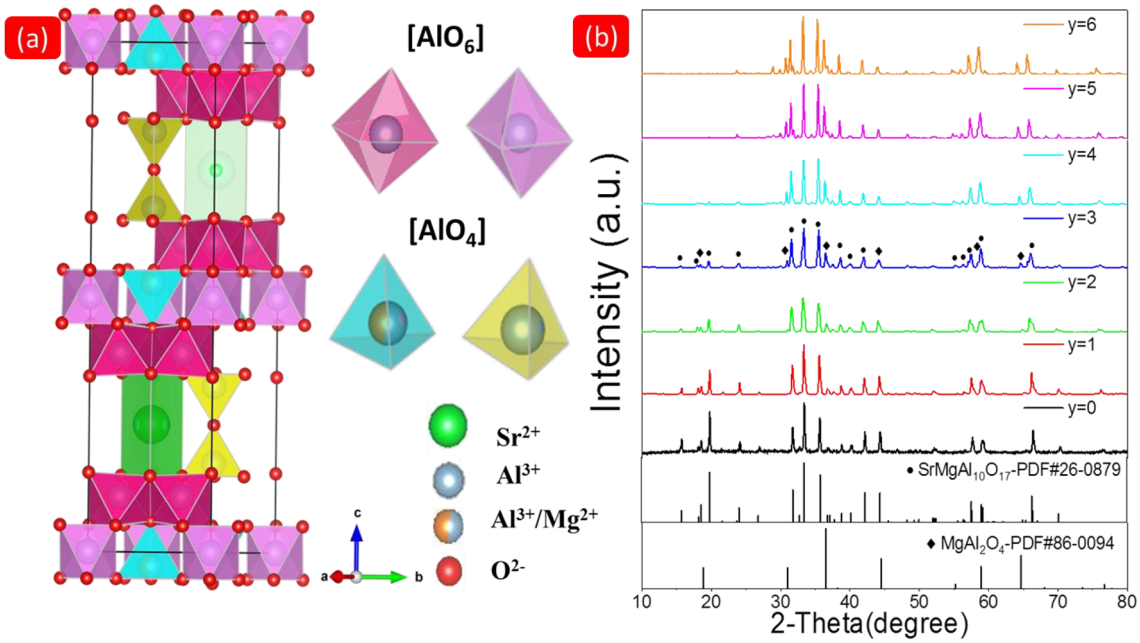

Fig. 1. (a) The crystal structure of $SrMgAl_{10}O_{17}$ host, the coordination environment of the octahedron [AlO_6] and tetrahedron [AlO_4]; (b) The XRD patterns of $SrMgAl_{10-y}Ga_yO_{17}$:1.0%Mn^{4+} (y = 0, 1, 2, 3, 4, 5, 6) phosphors.

PDF#26–0879. Considering the photoluminescence excitation (PLE) and emission (PL) spectra of samples with different content of flux, the emission intensity come to the maximum when 2 wt% H_3BO_3 participate in the synthesis reaction, and thus this condition is selected in the following section.

The $SrMgAl_{10}O_{17}$ crystal belongs to *P63/mmc* space group with hexagonal structure as shown in Fig. 1 (a). It is worth noting that the asymmetric part of the unit cell contains four independent sites of Al^{3+} which can be written as two [AlO_6] and two [AlO_4]. One type of Al^{3+} in tetrahedron [AlO_4] shares the position with Mg^{2+} randomly. In general, activator ion Mn^{4+} prefers to replace Al^{3+} in octahedron [AlO_6] position due to the similar ionic radius between Mn^{4+} (r = 0.530 Å, CN = 6) and Al^{3+} (r = 0.535 Å, CN = 6), and Mn^{4+} is more stable in octahedral environment with stronger ligand-field stabilization energy [31]. When a small quantity of Mn^{4+} replace Al^{3+} in the $SrMgAl_{10}O_{17}$ matrix, the XRD patterns keep the original position without any shift, the experimental results are shown in Fig. S2. Rietveld refinement analysis is performed in $SrMgAl_{10}O_{17}$:1.0%Mn^{4+} sample, and there are still two impurities phase $SrAl_2O_4$ and $MgAl_2O_4$, the contents of them are determined to be 6.38% and 7.50%. The cell parameters of this sample are listed as a = b = 5.62 Å, c = 22.41 Å and V = 614.25 $Å^3$, while these parameters in pure $SrMgAl_{10}O_{17}$ are a = b = 5.63 Å, c = 22.47 Å and V = 616.80 $Å^3$, indicates that Mn^{4+} is doped into the unit cell successfully. With more Ga^{3+} doped into the phosphor, the XRD curves exhibit complex phase gradually, as seen in Fig. 1 (b). The sample y = 0 match well with the standard card of $SrMgAl_{10}O_{17}$ at first, then $MgAl_2O_4$ appear and its content gradually increase. XRD pattern of the sample y = 3 shows two phases: $SrMgAl_{10}O_{17}$ and $MgAl_2O_4$, which are noted as ● and ◆ respectively. According to literature research, there is no report about Mn^{4+} luminescence property in single $MgAl_2O_4$ matrix. Wu et al [32] found that $MgAl_2O_4$:Mn^{4+} sample show no photoluminescence emission but $MgAl_2O_4$ phase have advantages on the luminescence performance of the $MgAl_2O_4/CaAl_{12}O_{19}$:$Mn^{4+}$ composite sample. Accordingly, combined with the experiment results, it can expect that a small amount of $MgAl_2O_4$ phase can enhance the luminescence properties of sample. With further increasing of Ga^{3+} dopant, the phase of samples are mainly composed of $SrMgAl_{10}O_{17}$ host, XAl_2O_4 (X = Mg^{2+}, Mn^{2+}) and Ga_2O_3, and it should be noticed that the latter three compounds have similar XRD pattern with almost the same peak position. Considering there is no octahedral coordination in these phases as suitable luminescence centers for Mn^{4+}, thus they have little effect on the luminescence properties of sample theoretically.

3.2. Photoluminescence properties of $SrMgAl_{10-y}Ga_yO_4$:xMn^{4+} phosphors

Fig. 2(a) and (c) exhibit the PLE (λ_{em} = 662 nm) and PL (λ_{ex} = 320 nm and λ_{ex} = 467 nm) spectra of $SrMgAl_{10}O_{17}$:xMn^{4+} phosphors. It is obvious that the excitation and emission intensities are increasing with a rising concentration of Mn^{4+} at first, both of them reach maximum when x = 1.0% and then decrease with more Mn^{4+} doping. For the purpose of researching the concentration quenching behavior of $SrMgAl_{10}O_{17}$:xMn^{4+} phosphor, the critical distance R_c is taken into account, whose value can be determined by the equation below [33,34]:

$$R_c \approx 2\left[\frac{3V}{4\pi x_c N}\right]^{1/3} \quad (1)$$

where V stands for the cell volume, x_c is the critical concentration of Mn^{4+} and N refers to the number of available sites occupied by Mn^{4+}, respectively. For $SrMgAl_{10}O_{17}$:1.0%Mn^{4+} phosphor, V = 614.25 $Å^3$, x_c = 0.010 and N = 2, and the R_c is calculated to be 38.86 Å. This value is much larger than 5 Å which corresponding to the interaction between activator ions, therefore, the concentration quenching of $SrMgAl_{10}O_{17}$:xMn^{4+} belongs to the multipolar-multipolar interaction which can be divided to be dipole–dipole (d–d), dipole–quadrupole (d–q), and quadrupole–quadrupole (q–q) interactions, respectively. They refer to different values of θ in the following formula, which is often used to reflect the interactions based on the Dexter's theory [35,36]:

$$\frac{I}{x} = k\left[1 + \beta(x)^{\theta/3}\right]^{-1} \quad (2)$$

where I and x mean the emission intensity and concentration of Mn^{4+} dopant, k and β refer to a certain excitation condition and specific matrix crystal, and θ = 6, 8, 10 refer to d–d, d–q, and q–q interactions, respectively.

The specific value of θ is usually obtained by the slope of the dependence of log(I/x) versus log (x). From the inset in Fig. 2(a), there are two fitting lines corresponding to 320 nm and 467 nm for the excitation

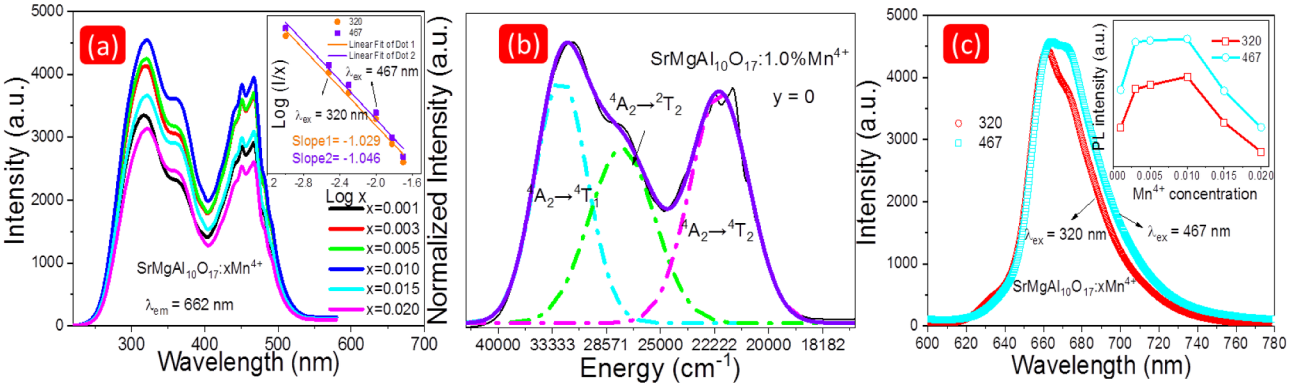

Fig. 2. (a) The photoluminescence excitation (PLE) spectra of $SrMgAl_{10}O_{17}:xMn^{4+}$ (x = 0.1%, 0.3%, 0.5%, 1.0%, 1.5%, 2.0%), and the inset is the dependence of log (I/x) versus log (x); (b) Gaussian fitting of $SrMgAl_{10}O_{17}$:1.0%Mn^{4+} sample; (c) The photoluminescence (PL) spectra of samples under the excitation of 320 nm and 467 nm respectively, and the inset is the tendency of emission intensity varies with Mn^{4+} doping concentration.

wavelength, two slopes are −1.029 and −1.046, respectively. The θ_1 and θ_2 are calculated to be 3.087 and 3.138, respectively, both of them are close to 6 which indicate the concentration quenching mechanism is dipole–dipole (d–d) interaction in $SrMgAl_{10}O_{17}:xMn^{4+}$ phosphor.

According to Fig. 2 (b), the PLE spectrum of $SrMgAl_{10}O_{17}$:1.0% Mn^{4+} is fitted into three Gaussian peaks located at 32468, 27472 and 22026 cm^{-1}, they are related to $^4A_2 \rightarrow {}^4T_1$, $^4A_2 \rightarrow {}^2T_2$ and $^4A_2 \rightarrow {}^4T_2$ transitions of Mn^{4+}, respectively. The PLE spectra of $SrMgAl_{10}O_{17}:xMn^{4+}$ phosphors have a large range from 220 to 580 nm, indicates that these phosphors can be easily excited by commercial blue and near-UV chips. Fig. 3(a) and (b) exhibit the photoluminescence excitation (PLE) and photoluminescence (PL) spectra of $SrMgAl_{10-y}Ga_yO_{17}$:1.0%Mn^{4+} samples. The intensity of PLE and PL spectra both increase with an incremental content of Ga^{3+} doping, and come to the maximum when $y = 3$. It is worth noting that the shape of PL spectrum changed significantly upon Ga^{3+} doping which related to a shift of the luminescence center. In the sample of $SrMgAl_{10}O_{17}$:1.0%Mn^{4+} (y = 0), the emission come from the Al center absolutely. When Ga^{3+} replace

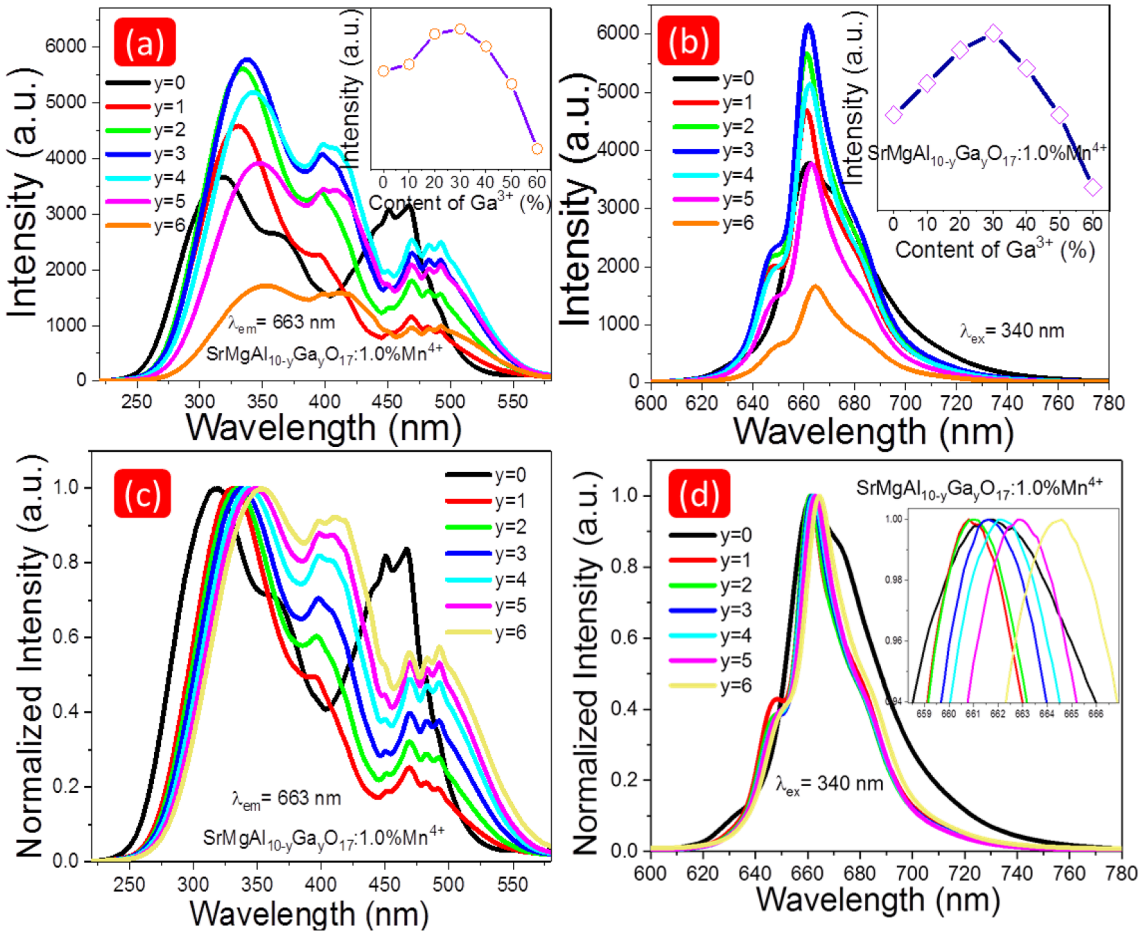

Fig. 3. (a) Photoluminescence excitation and (b) photoluminescence spectra of $SrMgAl_{10-y}Ga_yO_{17}$:1.0%Mn^{4+} (y = 0, 1, 2, 3, 4, 5, 6) phosphors; the normalized PLE spectra (c) monitored at 663 nm; the normalized PL spectra under (d) 340 nm excitation, and the insets are enlarged part of the peaks in the wavelength ranging from 658 to 668 nm.

Al^{3+} in samples from y = 1 to y = 6, new luminescence center of Ga site is generated, thus resulted in the change of spectra. Another interesting phenomenon is that the normalized PLE spectra exhibit obvious red shift as shown in Fig. 3 (c), that the $^4A_2 \rightarrow {}^2T_2$ transitions show a great enhancement and red shift with the increase of Ga^{3+} doping. Meanwhile, PL spectra excited at different wavelength all show slight red shift in Fig. 3 (d) and Fig. S4.

Based on this situation, crystal field theory and nephelauxetic effect are employed to explain these phenomena. There are three parameters to assess the effect of crystal field on the luminescent properties of Mn^{4+} that are described as the crystal-field parameter (D_q), Racah parameters (B) and (C), respectively. They are directly related to the PLE and PL spectra, and the values of D_q, B and C can be calculated from following equations [30,37]:

$$D_q = \frac{E(^4A_2 - {}^4T_2)}{10} \tag{3}$$

$$\frac{D_q}{B} = \frac{15(x-8)}{(x^2-10x)} \tag{4}$$

$$x = \frac{E(^4A_2 - {}^4T_1) - E(^4A_2 - {}^4T_2)}{D_q} \tag{5}$$

$$\frac{E(^2E_g - {}^4A_2)}{B} = \frac{3.05C}{B} + 7.9 - \frac{1.8B}{D_q} \tag{6}$$

According to Fig. 2, the energy levels of $^4T_1$, $^4T_2$ and ^2E_g in $SrMgAl_{10}O_{17}$:1.0%Mn^{4+} are 32468, 22026 and 15110 cm^{-1}, and its D_q, B and C are calculated to be 2203, 1123 and 2423 cm^{-1}, respectively. The value of D_q/B is evaluated to be 2.1, means that Mn^{4+} is exposed in a weak crystal field in $SrMgAl_{10}O_{17}$ matrix. Meanwhile, with the concentration of Ga^{3+} dopant increasing from 10% to 60%, the values of D_q/B are determined to be 2.22, 2.23, 2.24, 2.35, 2.43 and 2.49 which reveal a strong crystal field [38]. However, the change of crystal field is not the main reason in the red shift of Mn^{4+} emission due to its characteristic parity-forbidden d-d transition, and the nephelauxetic effect takes the predominant role in the luminescence of Mn^{4+} in most oxide phosphors [39,40]. The nephelauxetic effect has an influence on the energy of parity-forbidden $^2E_g \rightarrow {}^4A_2$ transition of Mn^{4+}, which can be described by the following formula [41,42]:

$$\beta_1 = \sqrt{(\frac{B}{B_0})^2 + (\frac{C}{C_0})^2} \tag{7}$$

where B_0 and C_0 are the Racah parameters for free ions, and the values of them are B_0 = 1160 cm^{-1} and C_0 = 4303 cm^{-1} for Mn^{4+}, respectively. The details of these parameters about crystal field and nephelauxetic effect of $SrMgAl_{10-y}Ga_yO_{17}$:1.0%Mn^{4+} phosphors are listed in Table 1.

According to the Tanabe-Sugano energy-level diagram of Mn^{4+} as shown in Fig. 4, the energy of $^2E_g \rightarrow {}^4A_2$ transition of Mn^{4+} is mainly determined by the Racah parameter B which relates to chemical bonding between the Mn^{4+} and the ligand. In general, a weaken nephelauxetic effect in bonding has smaller Racah parameter B, and thus shift down energy scale of ^2E level [38,43], means it has lower energy.

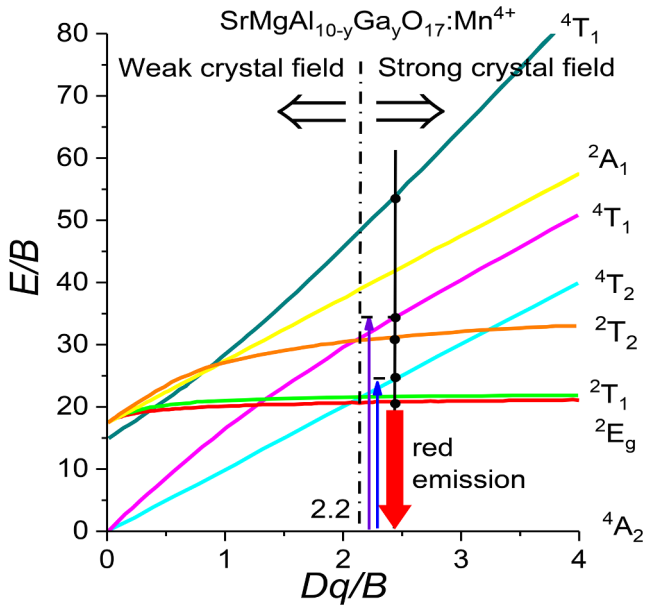

Fig. 4. Tanabe-Sugano energy-level diagram of Mn^{4+} in $SrMgAl_{10-y}Ga_yO_{17}$:1.0%Mn^{4+} phosphors.

Meanwhile, wavelength is inversely proportional to energy that can ascribe to λ = 1240/E, thus lower energy E results in longer wavelength, corresponding to red-shift phenomenon of the emission position. To sum up, a smaller value of the Racah parameter B gives the lower energy of $^2E_g \rightarrow {}^4A_2$ transition, corresponding to the red-shift phenomenon in the luminescence emission, and experimental results are in agreement with the theory.

Fig. 5(a) shows the diffuse reflection spectra of these powder samples, it is obvious that the reflection rate are decreasing with more content of Ga^{3+}, which has the same trend as a change of the PLE spectra. All diffuse reflection curves can be divided into four parts corresponding to the absorption of matrix and $^4A_2 \rightarrow {}^4T_1$, $^4A_2 \rightarrow {}^2T_2$, $^4A_2 \rightarrow {}^4T_2$ transitions of Mn^{4+}, respectively, which is consistent with the Gaussian fitting of PLE spectrum mentioned above. The diffuse reflection spectra can be translated into UV–vis absorption spectra, and get the band gap energy further through the following equation [44,45]:

$$(\alpha h\nu)^{1/2} = A(h\nu - E_g) \tag{8}$$

where α and A stand for the absorption parameter and proportional constant, $h\nu$ and E_g refer to the photon energy and the band gap, respectively. The band gap energy of this series samples increases from 5.25 eV to 5.44 eV and then drops down to 5.21 eV, as shown in Fig. 5 (b).

For the purpose of investigating the luminescence kinetics in $SrMgAl_{10-y}Ga_yO_{17}$:Mn^{4+} phosphors, the lifetime of these samples are measured and displayed in Fig. 6 (a). All of these curves fit well with the double-exponential decay model, see the following formula [46]:

Table 1
Energy States, crystal field parameters and calculated values of β_1 in $SrMgAl_{10-y}Ga_yO_{17}$:1.0%Mn^{4+} (y = 0, 1, 2, 3, 4, 5, 6) phosphors.

Sample	$^4A_2 \rightarrow {}^4T_1$ (cm^{-1})	$^4A_2 \rightarrow {}^4T_2$ (cm^{-1})	$^2E_g \rightarrow {}^4A_2$ (cm^{-1})	D_q	B	C	D_q/B	β_1
y = 0	32468	22026	15110	2203	1123	2423	1.96	1.120
y = 1	30303	21097	15133	2110	951	2797	2.22	1.046
y = 2	29940	20877	15129	2088	935	2833	2.23	1.040
y = 3	29674	20704	15115	2070	924	2852	2.24	1.036
y = 4	29240	20619	15106	2062	876	2952	2.35	1.020
y = 5	28986	20576	15088	2058	847	3008	2.43	1.011
y = 6	28653	20450	15047	2045	821	3051	2.49	1.002

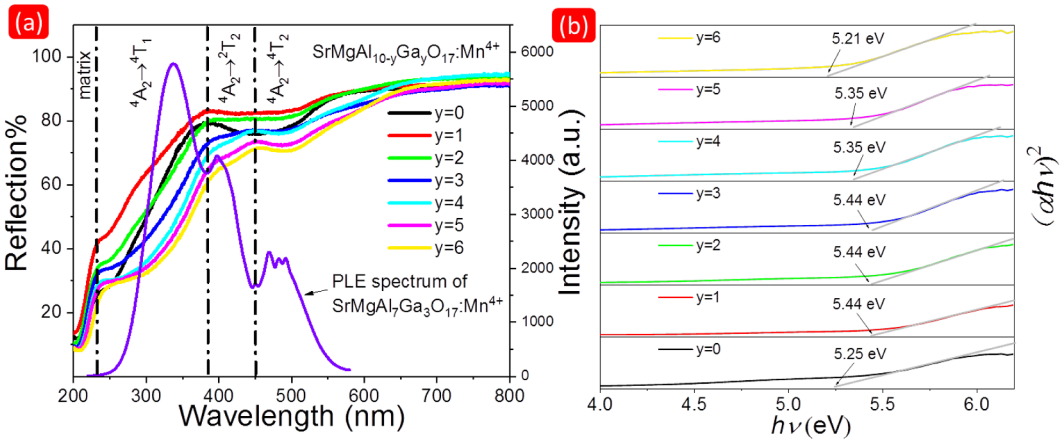

Fig. 5. (a) The diffuse reflection spectra of $SrMgAl_{10-y}Ga_yO_{17}$:1.0%Mn^{4+} phosphors and one PLE spectrum of $SrMgAl_7Ga_3O_{17}$:1.0%Mn^{4+} sample; (b) the corresponding band gap energy fitting.

$$I(t) = I_0 + C_1\exp(-t/\tau_1) + C_2\exp(-t/\tau_2) \quad (9)$$

And the average lifetime$\tau_{ave.}$ can be further calculated as [47]:

$$\tau_{ave.} = \frac{C_1\tau_1^2 + C_2\tau_2^2}{C_1\tau_1 + C_2\tau_2} \quad (10)$$

where I and I_0 stand for the photoluminescence intensity at time t and 0, C_1 and C_2 refer to pre-exponential factors, τ_1 and τ_2 are the lifetime components, respectively. The average lifetimes of $SrMgAl_{10-y}Ga_yO_{17}:Mn^{4+}$ are calculated to be 0.446, 0.476, 0.383, 0.320, 0.266, 0.207 and 0.126 ms when the Ga^{3+} dopant increased from 0 to 60%. Details about fitting information of the decay times are shown in the Table S1. The double-exponential decay model indicates that Mn^{4+} should have two luminescence centers in $SrMgAl_{10-y}Ga_yO_{17}$ matrix, which is consistent with the emission spectra.

Quantum efficiency (QE) is an important parameter to evaluate luminescence property of phosphors, the internal quantum efficiency (IQE) of $SrMgAl_7Ga_3O_{17}:Mn^{4+}$ and $SrMgAl_{10}O_{17}:Mn^{4+}$ samples are shown in Fig. 6 (b) and Fig. S5, which can be calculated via the following formula [48,49]:

$$\eta = \frac{\int L_S}{\int E_R - \int E_S} \quad (11)$$

herein, η is internal quantum efficiency, L_S stands for the luminescence spectra of the sample, E_R and E_S refer to the excitation line of $BaSO_4$ reference and sample, respectively. The IQE of $SrMgAl_7Ga_3O_{17}:Mn^{4+}$ and $SrMgAl_{10}O_{17}:Mn^{4+}$ are determined to be 29.67% and 51.40%. These values of the samples are at a moderate level compared to other red or deep red phosphors that have been reported such as $SrLaScO_4:Mn^{4+}$ (IQE: 12.2%) [50], $NaGdCa_4W_2O_{12}:Mn^{4+}$ (21.0%) [51], $SrAl_3BO_7:Mn^{4+}$ (26.0%) [52], $Ba_2YNbO_6:Mn^{4+}$ (IQE: 29.2%) [53], $Ca_2LaSbO_6:Mn^{4+}$ (IQE: 52.2%) [54]. Nevertheless, the photoluminescence properties of $SrMgAl_{10-y}Ga_yO_{17}:Mn^{4+}$ phosphors are expected to improve via further modification process likes charge compensation or energy transfer with co-doping sensitizer ion.

Fig. 7 (a) and (b) are the temperature-dependence luminescence spectra to evaluate the thermal stability of phosphor. The emission intensity decreases rapidly as the temperature increasing in both of the two samples, and the decline trend is more serious in $SrMgAl_7Ga_3O_{17}:Mn^{4+}$ phosphor. It because that Ga^{3+} doping destroys the stability of matrix structure to some extent and leads to lower activation energy, promotes the loss of energy with non-radiative processes and results in worse thermal stability. Therefore, thermal stability of this phosphor needs to be further improved through modifications such as coating and synthesis optimization to fit further applications.

Fig. 8 shows the mechanism diagram in $SrMgAl_9GaO_{17}:Mn^{4+}$ and $SrMgAl_4Ga_6O_{17}:Mn^{4+}$ for clearly describing the energy transition process. There is only Mn^{4+} ion transition emission in these phosphors,

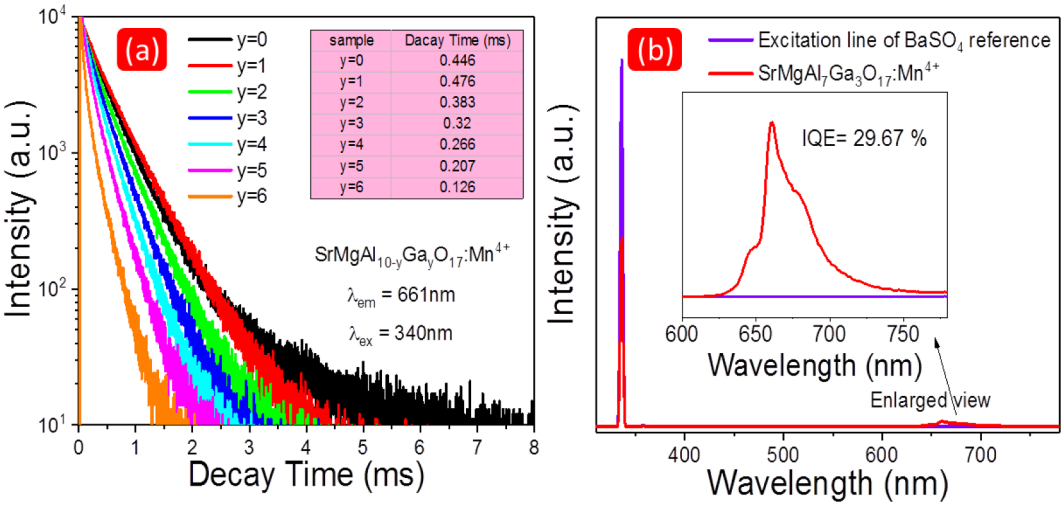

Fig. 6. (a) The lifetime decay curves of $SrMgAl_{10-y}Ga_yO_{17}$:1.0%Mn^{4+} phosphors monitored at 661 nm; the measurement of quantum efficiency of (b) $SrMgAl_7Ga_3O_{17}$:1.0%Mn^{4+}, and the insets are the enlarged pattern ranging from 600 nm to 780 nm.

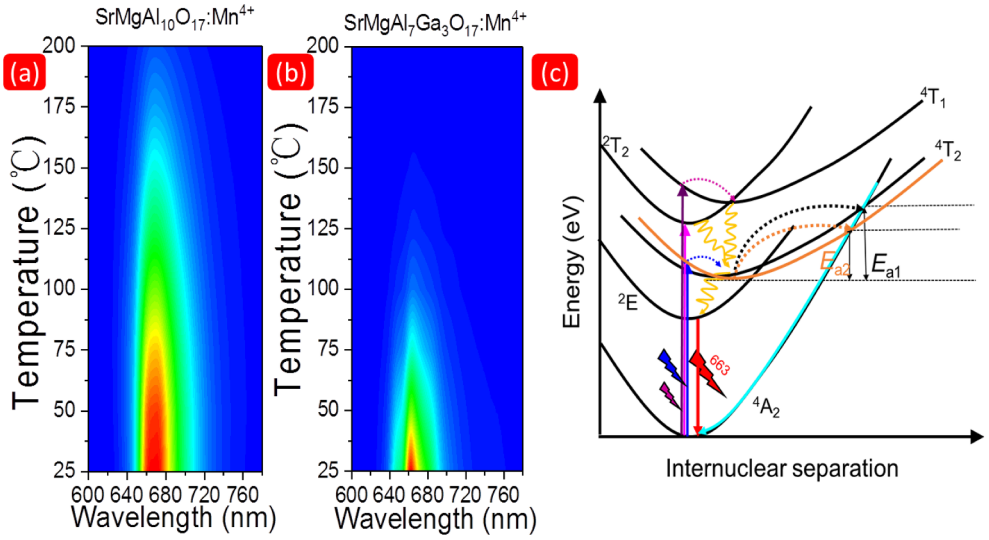

Fig. 7. The temperature-dependence luminescence spectrum of (a) $SrMgAl_{10}O_{17}$:1.0%Mn^{4+} and (b) $SrMgAl_7Ga_3O_{17}$:1.0%Mn^{4+}; (c) configurational coordinate diagram for Mn^{4+} ions in $SrMgAl_{10-y}Ga_yO_{17}$ phosphor.

electron is excited from $^4A_2$ energy level to $^4T_1$, $^4T_2$ and even conduction band, and then relaxes to ^2E_g level through non-radiative transition process, finally transfers to $^4A_2$ level with bright red emission. According to the results calculated above, the sample with more Ga^{3+} dopant has lower energy in the $^4T_1$, $^4T_2$ and ^2E_g states, and the energy of $^2E_g \rightarrow {}^4A_2$ transition directly decide the position of red emission. Therefore, there is an obvious red shift on the PLE and PL spectra with more content of Ga^{3+} in $SrMgAl_{10-y}Ga_yO_{17}$:Mn^{4+} phosphors.

3.3. The emission property of as-obtained LED device

In order to search for the potential application of $SrMgAl_{10-y}Ga_yO_{17}$:Mn^{4+} phosphor, LED devices are fabricated with 470 nm blue chips and different content of the as-obtained $SrMgAl_7Ga_3O_{17}$:Mn^{4+} sample, the emission spectra are shown in Fig. 9 (a) and (b). The red emission continues rising with an increasing content of phosphor, indicates that the ratio of blue and red light can be easily adjusted to meet the needs of different plants growth. The CIE chromaticity coordinates of these device change from (0.1456, 0.0365) to (0.5776, 0.2291), that from blue light to red light. Other four chromaticity coordinates with different content of the phosphor are (0.1852, 0.0603), (0.2149, 0.0754), (0.3391, 0.1256), and (0.4578, 0.1782), respectively. The emission spectrum of the fabricated LED device with appropriate phosphor is mainly composed of the blue band (420–500 nm) and red band (650–750 nm) with the peak at 470 nm and 663 nm, which can fit the absorption spectra of plant pigment including chlorophyll *A*, B and phytochrome P_R, P_{FR}, indicates that the $SrMgAl_{10-y}Ga_yO_{17}$:Mn^{4+} phosphors can be a candidate for plant growth LED light.

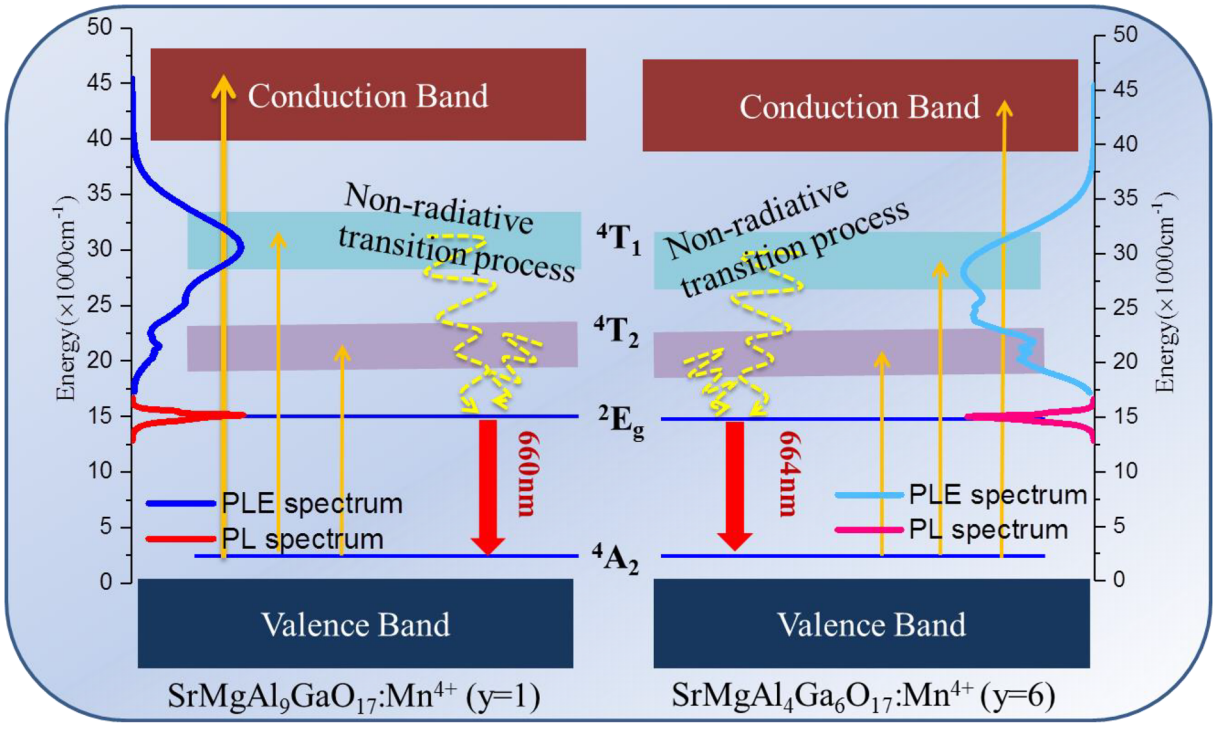

Fig. 8. Mechanism diagram of luminescence in $SrMgAl_9GaO_{17}$:1.0%Mn^{4+} and $SrMgAl_4Ga_6O_{17}$:1.0%Mn^{4+} phosphors.

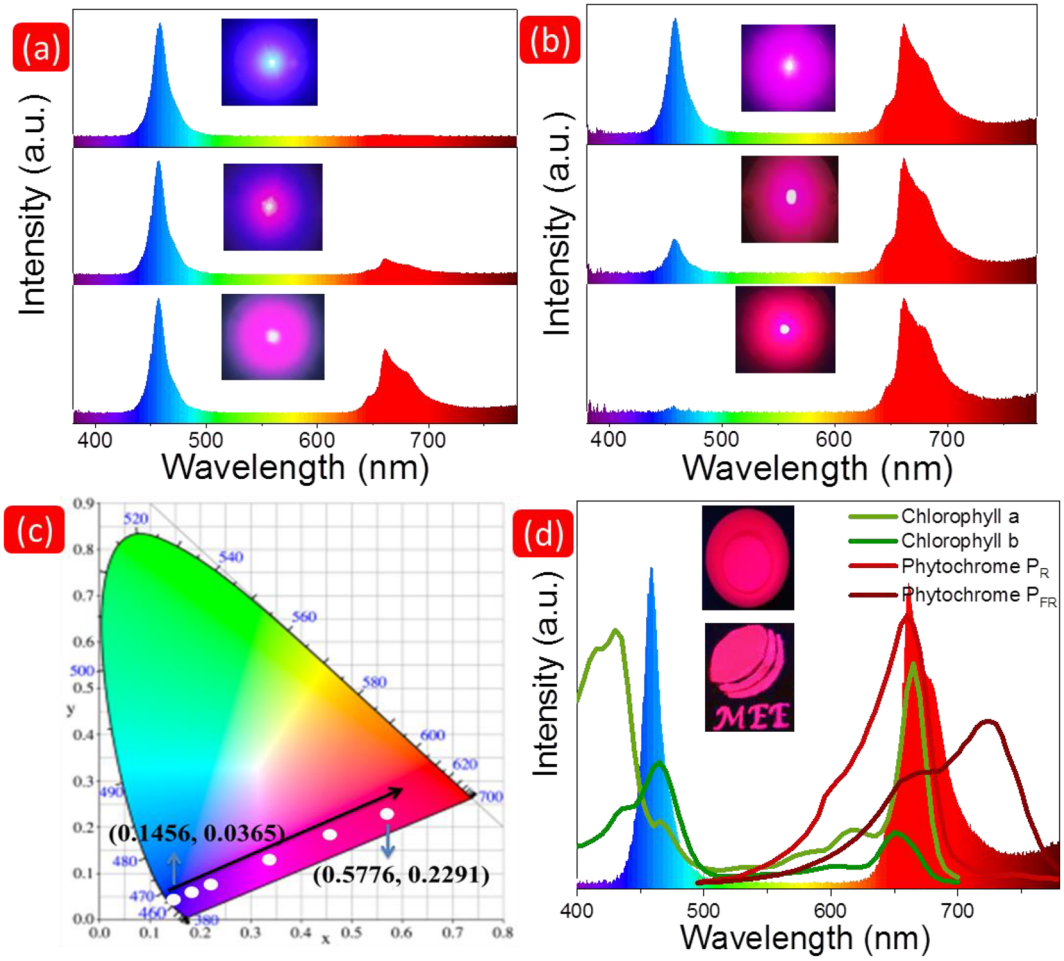

Fig. 9. (a) (b) Emission spectra of the fabricated LEDs combined with 470 nm blue chip and different contents of $SrMgAl_7Ga_3O_{17}$:1.0%Mn^{4+} sample, and the insets are the photos of the device; (c) CIE chromaticity diagram of LED devices; (d) the comprehensive comparison between emission spectra of device and the absorption curves of the plant pigments of Chlorophyll *A*, *B* and phytochrome P_R, P_{FR}. (For interpretation of the references to colour in this figure legend, the reader is referred to the web version of this article.)

4. Conclusions

In this work, a series of novel $SrMgAl_{10-y}Ga_yO_{17}$:xMn^{4+} red phosphors with enhanced and tunable luminescence properties were synthesized through high temperature approach. An appropriate amount of Ga^{3+} dopant improves the luminescent intensity to 163% in $SrMgAl_7Ga_3O_{17}$:Mn^{4+} sample compared to the original $SrMgAl_{10}O_{17}$:Mn^{4+} phosphor and causes the red shift in photoluminescence excitation (PLE) and photoluminescence (PL) spectra. The red shift observed in the spectra is explained by crystal field theory and nephelauxetic effect. All samples have a broad band in the PLE spectra ranging from 220 to 580 nm indicates they can be excited by both near ultraviolet and blue chips. The Ga^{3+} dopant increases the band gap of $SrMgAl_7Ga_3O_{17}$:Mn^{4+} sample to reduce non-radiative transitions and improve the emission intensity but leads to worse thermal stability for its low activation energy. Devices assembled with blue chip and the as-obtained $SrMgAl_7Ga_3O_{17}$:Mn^{4+} phosphor emits bright blue and red light which match the plant absorption spectra well, thus the $SrMgAl_{10-y}Ga_yO_{17}$:Mn^{4+} phosphor have potential application on plant growth LED light.

Declaration of competing interests

The authors declare that they have no known competing financial interests or personal relationships that could have appeared to influence the work reported in this paper.

Acknowledgements

The authors would like to gratefully acknowledge funds from the National Natural Science Foundation of China (Grant No. 21706060, 51703061, 51974123), the Hunan Graduate Research and Innovation Project (Grant No. CX2018B396), the Hunan provincial Engineering Technology Research Center for Optical Agriculture (Grant No. 2018TP2003), the Scientific Research Fund of Hunan Provincial Education Department (15K058, 19C0903), the Natural Sciences Foundation of Hunan agricultural university, China (Grant No. 19QN11), Science and Technology project of Changsha (KH1801219), Huxiang high level talent gathering project (2019RS1077), Double first-class construction project of Hunan Agricultural University (SYL201802002&SYL201802002). L. Liu thanks the National Natural Science Foundation of China (21671061) and application foundation frontier special project by Wuhan Science and Technology Bureau (2019010701011414) for the support of this work. W.-Y. Wong acknowledges the financial support from the Hong Kong Research Grants Council (C4006-17G and PolyU 153058/19P), the Hong Kong Polytechnic University (1-ZE1C) and Ms Clarea Au for the Endowed Professorship in Energy (847S).

Appendix A. Supplementary data

Supplementary data to this article can be found online at https://doi.org/10.1016/j.cej.2020.125208.

References

[1] T. Nakajima, T. Tsuchiya, Plant habitat-conscious white light emission of Dy^{3+} in whitlockite-like phosphates: reduced photosynthesis and inhibition of bloom impediment, ACS Appl. Mater. Interfaces 7 (2015) 21398–21407.

[2] M.R. Sabzalian, P. Heydarizadeh, M. Zahedi, A. Boroomand, M. Agharokh, M.R. Sahba, B. Schoefs, High performance of vegetables, flowers, and medicinal plants in a red-blue LED incubator for indoor plant production, Agron. Sustainable Dev. 34 (2014) 879–886.

[3] L. Poulet, G.D. Massa, R.C. Morrow, C.M. Bourget, R.M. Wheeler, C.A. Mitchell, Significant reduction in energy for plant-growth lighting in space using targeted LED lighting and spectral manipulation, Life Sci. Space Res. 2 (2014) 43–53.

[4] J. Zhang, W. Zhou, X. Ji, W. Ma, Z. Qiu, L. Yu, C. Li, Z. Xia, Z. Wang, S. Lian, Composition screening in blue-emitting $Li_4Sr_{1+x}Ca_{0.97}x(Si_O4_)2$: $^{Ce}3+$ phosphors for high quantum efficiency and thermally stable photoluminescence, ACS Appl. Mater. Interfaces 9 (2017) 30746–30754.

[5] Z. Zhou, Y. Zhong, M. Xia, N. Zhou, B.F. Lei, J. Wang, F.F. Wu, Tunable dual emission of $Ca_3Al_4ZnO_{10}:Bi^{3+}$, $M^{n4}+$ via energy transfer for indoor plant growth lighting, J. Mater. Chem. C 6 (2018) 8914–8922.

[6] R. Cao, T. Chen, Y. Ren, T. Chen, H. Ao, W. Li, G. Zheng, Synthesis and photoluminescence properties of $Ca_2LaTaO_6:Mn^{4+}$ phosphor for plant growth LEDs, J. Alloys Compd. 780 (2019) 749–755.

[7] J. Li, J. Yan, D. Wen, W.U. Khan, J. Shi, M. Wu, Q. Su, P.A. Tanner, Advanced Red Phosphors for White Light-emitting Diodes, J. Mater. Chem. C 4 (2016) 8611–8623.

[8] F. Hong, H. Xu, L. Yang, G. Liu, C. Song, X. Dong, W. Yu, Mn^{4+} nonequivalent doping Al^{3+}-based cryolite high-performance warm WLED red phosphors, New J. Chem. 43 (2019) 14859–14871.

[9] J. He, C. Yan, M. Huang, R. Shi, Y. Chen, C.D. Ling, Z.Q. Liu, Mechanistic insight into energy transfer dynamics and color tunability of $Na_4CaSi_3O_9:Tb^{3+}$, Eu^{3+} for warm white LEDs, Chem. Eur. J. (2020), https://doi.org/10.1002/chem.201905607.

[10] Y. Chen, K. Wu, J. He, Z. Tang, J. Shi, Y. Xu, Z.Q. Liu, A bright and moisture-resistant red-emitting $Lu_3Al_5O_{12}$: Mn^{4+}, Mg^{2+} garnet phosphor for high-quality phosphor-converted white LEDs, J. Mater. Chem. C 5 (2017) 8828–8835.

[11] J. Ueda, K. Kuroishi, S. Tanabe, Bright persistent ceramic phosphors of Ce^{3+}-Cr^{3+}-codoped garnet able to store by blue light, Appl. Phys. Lett. 104 (2014) 101904.

[12] H.R. Abd, Z. Hassan, N.M. Ahmed, F.H. Alsultany, A.F. Omar, Ce-doped YAG phosphor powder synthesized via microwave combustion and its application for white LED, Opt. Eng. 58 (2019) 181416–181423.

[13] X.Q. Piao, K. Machida, T. Horikawa, H. Hanzawa, Y. Shimomura, N. Kijima, Preparation of $CaAlSiN_3:Eu^{2+}$ phosphors by the self-propagating high-temperature synthesis and their luminescent properties, Chem. Mater. 19 (2007) 4592–4599.

[14] J.W. Li, T. Watanabe, H. Wada, T. Setoyama, M. Yoshimura, Low-temperature crystallization of Eu-doped red-emitting $CaAlSiN_3$ from alloy-derived ammonometallates, Chem. Mater. 19 (2007) 3592–3594.

[15] Y.T. Tsai, C.Y. Chiang, W. Zhou, J.F. Lee, H.S. Sheu, R.S. Liu, Structural ordering and charge variation induced by cation substitution in (Sr, Ca)$AlSi_N$3: Eu phosphor, J. Am. Chem. Soc. 137 (2015) 8936–8941.

[16] Y.Q. Li, J.E.J. van Steen, J.W.H. van Krevel, G. Botty, A.C.A. Delsing, F.J. DiSalvo, G. de With, H.T. Hintzen, Luminescence properties of red-emitting $M_2Si_5N_8:Eu^{2+}$ (M = Ca, Sr, Ba) LED conversion phosphors, J. Alloys Compd. 417 (2006) 273–279.

[17] Y.Q. Li, G. de With, H.T. Hintzen, The effect of replacement of Sr by Ca on the structural and luminescence properties of the red-emitting $Sr_2Si_5N_8:Eu^{2+}$ LED conversion phosphor, J. Solid State Chem. 181 (2008) 515–524.

[18] M.H. Fang, C.S. Hsu, C. Su, W. Liu, Y.H. Wang, R.S. Liu, Integrated surface modification to enhance the luminescence properties of $K_2TiF_6:Mn^{4+}$ phosphor and its application in white-light-emitting diodes, ACS Appl. Mater. Interfaces 10 (2018) 29233–29237.

[19] L. Huang, Y. Liu, J. Yu, Y. Zhu, F. Pan, T. Xuan, M.G. Brik, C. Wang, J. Wang, Highly stable $K_2SiF_6:Mn^{4+}$@K_2SiF_6 composite phosphor with narrow red emission for white LEDs, ACS Appl. Mater. Interfaces 10 (2018) 18082–18092.

[20] Q. Zhou, L. Dolgov, A.M. Srivastava, L. Zhou, Z. Wang, J. Shi, M.D. Dramićanin, M.G. Brik, M. Wu, Mn^{2+} and Mn^{4+} red phosphors: synthesis, luminescence and applications in WLEDs. A review, J. Mater. Chem. C 6 (2018) 2652–2671.

[21] Z. Zhou, N. Zhou, M. Xia, Y. Meiso, H.T. (Bert) Hintzen, Research progress and application prospect of transition metal Mn^{4+}-activated luminescent materials, J. Mater. Chem. C 4 (2016) 9143–9161.

[22] K. Sankarasubramanian, B. Devakumar, G. Annadurai, L. Sun, Y.J. Zeng, X.Y. Huang, Novel $SrLaAlO_4:Mn^{4+}$ deep-red emitting phosphors with excellent responsiveness to phytochrome PFR for plant cultivation LEDs: synthesis, photoluminescence properties, and thermal stability, RSC Adv. 8 (2018) 30223–30229.

[23] L. Sun, B. Devakumar, J. Liang, B. Li, S. Wang, Q. Sun, H. Guo, X. Huang, Thermally stable $La_2LiSbO_6:Mn^{4+}$, $M^{g2}+$ far-red emitting phosphors with over 90% internal quantum efficiency for plant growth LEDs, RSC Adv. 8 (2018) 31835–31842.

[24] J. Xiang, J. Chen, N. Zhang, H. Yao, C.F. Guo, Far red and near infrared double-wavelength emitting phosphor Gd_2ZnTiO_6: Mn^{4+}, $Y^{b3}+$ for plant cultivation LEDs, Dyes Pigm. 154 (2018) 257–262.

[25] J. Chen, W. Zhao, N. Wang, Y. Meng, S. Yi, J. He, X. Zhang, Energy transfer properties and temperature-dependent luminescence of $Ca_{14}Al_{10}Zn_6O_{35}$: Dy^{3+}, Mn^{4+} phosphors, J. Mater. Sci. 51 (2016) 4201–4212.

[26] Z. Zhou, Y. Li, M. Xia, Y. Zhong, N. Zhou, H.T. (Bert) Hintzenc, Improved luminescence and energy-transfer properties of $Ca_{14}Al_{10}Zn_6O_{35}:Ti^{4+}$, $M^{n4}+$ deep-red-emitting phosphors with high brightness for light-emitting diode (LED) plant-growth lighting, Dalton Trans. 47 (2018) 13713–13721.

[27] Y. Zhou, W. Zhao, C. Lu, Z. Liao, Synthesis and luminescence properties of Mn^{4+}-dopant $Ca_{14}Zn_6Ga_{10-x}Al_xO_{35}$ solid solution, Prog. Nat. Sci.: Mater. Int. 28 (2018) 301–307.

[28] Z. Zhou, M. Xia, Y. Zhong, S. Gai, S. Huang, Y. Tian, X.Lu.N. Zhou, Dy^{3+}@Mn^{4+} co-doped $Ca_{14}Ga_{10-m}Al_mZn_6O_{35}$ far-red emitting phosphors with high brightness and improved luminescence and energy transfer properties for plant growth LED lights, J. Mater. Chem. C 5 (2017) 8201–8210.

[29] J. Qiao, Z. Zhang, J. Zhao, Z. Xia, Tuning of the compositions and multiple activator sites toward single-phased white emission in $(Ca_{9-x}Sr_x)MgK(PO_4)_7:Eu^{2+}$ phosphors for solid-state lighting, Inorg. Chem. 58 (2019) 5006–5012.

[30] J. Long, Y. Wang, R. Ma, C. Ma, X. Yuan, Z. Wen, M. Du, Y. Cao, Enhanced luminescence performances of tunable $Lu_{3-x}Y_xAl_5O_{12}:Mn^{4+}$ red phosphor by ions of Rn^+ (Li^+, Na^+, Ca^{2+}, Mg^{2+}, Sr^{2+}, Sc^{3+}), Inorg. Chem. 56 (2017) 3269–3275.

[31] W. Xu, D. Chen, S. Yuan, Y. Zhou, S. Li, Tuning excitation and emission of Mn^{4+} emitting center in $Y_3Al_5O_{12}$ by cation substitution, Chem. Eng. J. 317 (2017) 854–861.

[32] Y. Wu, Y. Zhuang, R.J. Xie, K. Ruan, X. Ouyang, A novel Mn^{4+} doped red phosphor composed of $MgAl_2O_4$ and $CaAl_{12}O_{19}$ phases for light-emitting diodes, Dalton Trans. 49 (2020) 3606–3614.

[33] P.A.M. Berdowski, G. Blasse, Luminescence and energy transfer in a highly symmetrical system: $Eu_2Ti_2O_7$, J. Solid State Chem. 62 (1986) 317–327.

[34] G. Blasse, Energy transfer in oxidic phosphors, Phys. Lett. A 28 (1968) 444–445.

[35] D.L. Dexter, A theory of sensitized luminescence in solids, J. Chem. Phys. 21 (1953) 836–850.

[36] D.L. Dexter, J.H. Schulman, Theory of concentration quenching in inorganic phosphors, J. Chem. Phys. 22 (1954) 1063–1070.

[37] Y. Zhong, S. Gai, M. Xia, S. Gu, Y. Zhang, X. Wu, J. Wang, N. Zhou, Z. Zhou, Enhancing quantum efficiency and tuning photoluminescence properties in far-red-emitting phosphor $Ca_{14}Ga_{10}Zn_6O_{35}:Mn^{4+}$ based on chemical unit engineering, Chem. Eng. J. 374 (2019) 381–391.

[38] C. Jiang, X. Zhang, J. Wang, Q. Zhao, K.L. Wong, M. Peng, Synthesis and photoluminescence properties of a novel red phosphor $SrLaGaO_4:Mn^{4+}$, J. Am. Ceram. Soc. 102 (2019) 1269–1276.

[39] M.G. Brik, A.M. Srivastava, On the optical properties of the Mn^{4+} ion in solids, J. Lumin. 133 (2013) 69–72.

[40] S. Adachi, Photoluminescence properties of Mn^{4+} -activated oxide phosphors for use in white-LED applications: A review, J. Lumin. 202 (2018) 263–281.

[41] F. Hong, L. Yang, H. Xu, Z. Chen, Q. Liu, G. Liu, X. Dong, W. Yu, A red-emitting Mn^{4+} activated phosphor with controlled morphology and two-dimensional luminescence nanofiber film: Synthesis and application for high-performance warm white light-emitting diodes (WLEDs), J. Alloys Compd. 808 (2019) 151551.

[42] C. Tian, H. Lin, D. Zhang, P. Zhang, R. Hong, Z. Han, X. Qian, J. Zou, Mn^{4+} activated Al_2O_3 red-emitting ceramic phosphor with excellent thermal conductivity, Opt. Express 27 (2019) 32666–32678.

[43] M.H. Du, Chemical trends of Mn^{4+} emission in solids, J. Mater. Chem. C 2 (2014) 2475–2481.

[44] X. Wu, L. Liu, M. Xia, S. Huang, Y. Zhou, W. Hu, Z. Zhou, N. Zhou, Enhance the luminescence properties of $Ca_{14}Al_{10}Zn_6O_{35}:Ti^{4+}$ phosphor via cation vacancies engineering of Ca^{2+} and Zn^{2+}, Ceram. Int. 45 (2019) 9977–9985.

[45] M. Xia, S. Gu, C. Zhou, L. Liu, Y. Zhong, Y. Zhang, Z. Zhou, Enhanced photoluminescence and energy transfer performance of $Y_3Al_4GaO_{12}:Mn^{4+}$, $D^{y3}+$ phosphors for plant growth LED lights, RSC Adv. 9 (2019) 9244–9252.

[46] J. Hu, T. Huang, Y. Zhang, B. Lu, H. Ye, B. Chen, H. Xia, C. Ji, Enhanced deep-red emission from Mn^{4+}/Mg^{2+} co-doped $CaGdAlO_4$ phosphors for plant cultivation, Dalton Trans 48 (2019) 2455–2466.

[47] J. Zhou, Z. Xia, Luminescence color tuning of Ce^{3+}, Tb^{3+} and Eu^{3+} codoped and tri-doped $BaY_2Si_3O_{10}$ phosphors via energy transfer, J. Mater. Chem. C 3 (2015) 7552–7560.

[48] R. Cao, K.N. Sharafudeen, J. Qiu, Enhanced luminescence in $SrMgAl_xO_{17\pm d}$:yMn^{4+} composite phosphors, Spectrochim. Acta A Mol. Biomol. Spectrosc. 117 (2014) 402–405.

[49] S. Liu, P. Sun, Y. Liu, T. Zhou, S. Li, R.J. Xie, X. Xu, R. Dong, J. Jiang, H. Jiang, Warm white light with a high color-rendering index from a single $Gd_3Al_4GaO_{12}:Ce^{3+}$ transparent ceramic for high-power LEDs and LDs, ACS Appl. Mater. Interfaces 11 (2019) 2130–2139.

[50] U.B. Humayoun, S.N. Tiruneh, D.H. Yoon, On the crystal structure and luminescence characteristics of a novel deep red emitting $SrLaScO_4:Mn^{4+}$, Dyes Pigm. 152 (2018) 127–130.

[51] K. Li, R. Van Deun, Insight into emission-tuning and luminescence thermal quenching investigations in $NaLa_{1-x}Gd_xCa_4W_2O_{12}:Mn^{4+}$ phosphors via the ionic couple substitution of Na^+ + Ln^{3+} (Ln = La, Gd) for $2Ca^{2+}$ in $Ca_6W_2O_{12}:Mn^{4+}$ for plant-cultivation LED applications, Dalton Trans. 48 (2019) 15936–15941.

[52] Y. Zhong, N. Zhou, M. Xia, Y. Zhou, H. Chen, Z. Zhou, Synthesis and photoluminescence properties of novel red-emitting phosphor $SrAl_3BO_7:Mn^{4+}$ with enhanced emission by $Mg^{2+}/Zn^{2+}/Ca^{2+}$ incorporation for plant growth LED lighting, Ceram. Int. 45 (2019) 23528–23539.

[53] A. Fu, Q. Pang, H. Yang, L. Zhou, $Ba_2YNbO_6:Mn^{4+}$-based red phosphor for warm white light-emitting diodes (WLEDs): Photoluminescent and thermal characteristics, Opt. Mater. 70 (2017) 144–152.

[54] L. Shi, Y. Han, Z. Zhang, Z. Ji, D. Shi, X. Geng, H. Zhang, M. Li, Z. Zhang, Synthesis and photoluminescence properties of novel $Ca_2LaSbO_6:Mn^{4+}$ double perovskite phosphor for plant growth LEDs, Ceram. Int. 45 (2019) 4739–4746.